A Noninvasive Blood Glucose Estimation System Using Dual-Channel PPGs and Pulse-Arrival Velocity

Po-Lei Lee, *Member, IEEE*, Kuo-Wei Wang, and Chen-Yuan Hsiao

***Abstract*—Diabetes is a chronic metabolic disorder that requires individuals with diabetes to perform "finger stick blood sugar tests" multiple times a day. This invasive method is not capable of continuously monitoring a diabetic patient's blood glucose levels and can be painful and inconvenient in the long term. In our study, we developed a noninvasive blood glucose estimation method using dual-channel photoplethysmography (PPG) combined with pulse arrival velocity (PAV). The dual-channel PPG was chosen based on the advantages of 530 nm PPG in blood flow measurement and 1550 nm infrared light in blood glucose concentration detection. In addition to testing various amplitude features in PPG at different fiducial points (systolic peak, dicrotic notch, and diastolic peak), we also examined the amplitude ratio between the two PPG channels (530 nm green-light PPG and 1550 nm infrared PPG), as well as PAV, for noninvasive blood glucose estimation. In this study, we recruited 18 healthy subjects (14 males and four females; aged 29.4 ± 7.87 years old). The oral glucose tolerance test (OGTT) experiment was conducted on each participant to manipulate the blood glucose level. Each parameter for blood glucose estimation was examined using partial *F*-test to assess its impact on blood glucose estimation. We found that combining the amplitude ratio of the dual-channel PPG with PAV resulted in the best blood glucose estimation results, with estimation results falling within Zone A in the Clarke error grid analysis (CEGA) with a 100% success rate, and the root-mean-square-error (RMSE) being 7.46 ± 2.43 mg/dL.**

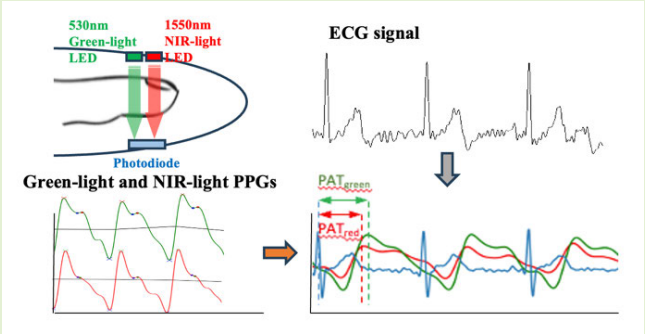

***Index Terms*— Blood glucose, dual-channel photoplethysmography (PPG), pulse arrival velocity (PAV).**

Manuscript received 17 July 2023; accepted 9 August 2023. Date of publication 23 August 2023; date of current version 2 October 2023. This work was supported in part by the National Science and Technology Council under Grant NSTC 111-2217-E-008-001-MY3, Grant 111-2221-E-008-102-MY3, Grant 111-2622-E-008-013, Grant 110-2923-E-008-002-MY3, and Grant 110-2221-E-008-095-MY3; and in part by the Taipei Medical University Project under Grant TMU111-AE1-B04. The associate editor coordinating the review of this article and approving it for publication was Dr. R. N. Ponnalagu. *(Corresponding author: Chen-Yuan Hsiao.)*

This work involved human subjects in its research. Approval of all ethical and experimental procedures and protocols was granted by the Ethics Committee of Institutional Review Board (IRB), Taoyuan Landseed Hospital, Taiwan, under Approval No. LSIHIRB: 21-003-A2.

Po-Lei Lee is with the Department of Electrical Engineering, National Central University, Taoyuan 32001, Taiwan (e-mail: pllee@ee.ncu.edu.tw).

Kuo-Wei Wang is with the Landseed International Hospital, Taoyuan 32449, Taiwan (e-mail: wangkw@landseed.com.tw).

Chen-Yuan Hsiao is with the Division of Cardiovascular Surgery, Department of Surgery, Taipei Medical University Hospital, Taipei 11031, Taiwan, also with the Taipei Heart Institute, Taipei Medical University, Taipei, Taiwan, and also with the Department of Surgery, School of Medicine, College of Medicine, Taipei Medical University, Taipei, Taiwan (e-mail: dreamsoar2005@gmail.com).

Digital Object Identifier 10.1109/JSEN.2023.3306343

I. Introduction

DIABETES is a chronic metabolic disorder caused by a lack of insulin production in a patient's pancreas or a lack of insulin absorption by cells. Prolonged diabetes can lead to other diseases, such as eye disorders, kidney disorders, heart diseases, and nerve disorders [1]. According to statistics from the World Health Organization, the number of diabetics will exceed 360 million by 2030. Once one is diagnosed with severe diabetes, the risk of admission to the intensive care unit (ICU) is 2.8 times higher than that of non-diabetic patients, and the mortality rate is eight times higher [1]. To keep track of patients' blood glucose levels, individuals with diabetes must perform "finger stick blood sugar tests" multiple times per day. This involves pricking their fingertips with a small needle to produce a blood drop on a test strip, which is then analyzed by a glucose meter to display the patient's blood sugar level. This invasive method is not able to continuously monitor a diabetic patient's blood glucose levels and can be painful and inconvenient in the long term. Accordingly, several research teams have focused their efforts in the past on creating noninvasive methods for continuously monitoring individuals' blood

glucose levels. Arnold [2] discovered the absorption degree of glucose solution on near-infrared spectroscopy and proposed the potential use of near-infrared spectroscopy to detect blood glucose according to the absorption coefficient of near-infrared light for glucose. Heise et al. [3] proposed near-infrared diffuse reflectance spectroscopy to detect blood glucose. Enejder et al. [4], [5] studied blood glucose using Raman spectroscopy with 830 nm light, and proposed the potential of using near-infrared light to detect blood glucose levels. Jean et al. [6] used microwaves to measure blood glucose, based on detecting the fluctuation of capacitance caused by blood glucose changes in the human body. Kulik et al. [7] utilized two multiplexed fiber-optic sensors to measure brachial–ankle pulse-wave velocity (PWV) and concluded PWV could be a potential approach for noninvasive blood glucose detection.

In recent years, infrared photoplethysmography (PPG) has been considered a highly potential noninvasive optical technology for blood glucose monitoring. Garcia-Carretero et al. [8] adopted the K-nearest neighborhood for measured PPG signals to binarily classify diabetics from normal subjects and had achieved 97% detection accuracy. Zhang et al. [9] used the Gaussian mixture model (GMM) to obtain features from PPG signals captured by chromatic camera, and support vector machine (SVM) was adopted for three-level blood glucose classification with 81.49% of detection accuracy. Habbu et al. [10] measured the feature of total power in PPG. The value of blood glucose was predicted using multilayer perceptron (MLP), and the proportion of 80.6% of the predicted values falling in Zone A on the Clarke error grid analysis (CEGA). Philip et al. [11] detected multi-PPG features, such as pulse area, variance entropy, and Kaiser–Teager energy, with predicted errors ranging from 6.5% to 13%. Al-Dhaheri et al. [12] used univariate linear regression to predict blood glucose levels based on PPG amplitude of systolic peaks, with an average RMSE of 10.44 mg/dL. In addition, with the rapid advancements in smartphone technology, many studies have been tried to conduct noninvasive blood glucose using visible-light camera from smart phones, instead of using infrared lights. Zhang et al. [9] used RGB chromatic camera to detect PPG signals and defined 22 PPG parameters to roughly classify a subject's blood glucose into three levels: normal ($<$200 mg/dL), borderline (250–300 mg/dL), and hyperglycemia ($>$300 mg/dL), with an accuracy of 81.49%. Islam et al. [13] measured visible light PPG signals on a smartphone and applied principal component regression (PCR), partial least square (PLS), and support vector regression (SVR) to analyze five PPG parameters (including peak value, peak-to-peak time interval, first derivative peak, and second derivative peak), with a measurement error of less than 17.02 mg/dL.

In the above studies, to noninvasively estimate subjects' blood glucose levels with optical measurement approaches, near-infrared light sources between 750–2500 nm have been proposed in previous literatures, due to their advantages of high penetration in skin and simple and affordable equipment compared to other optical methods. Among these NIR wavelengths, two overtone bands, the first (1400–2050 nm) and the second (750–1550 nm) absorption bands, are preferred due to their strong absorption responses to glucose bonds (C–H, O–H) [12]. Especially, the short-wave near infrared (NIR) range (i.e., the 750–1550 nm) have relatively small absorption coefficients in water, so NIR lights are less interfered by water contents. However, the NIR range between 750 and 950 nm, which is sensitive to the levels of hemoglobin and deoxy-hemoglobin, could be affected by changes in blood oxygen concentration and lead to errors in blood glucose measurement [14]. Therefore, the NIR wavelength close to 1550 nm is usually favored for blood glucose measurement [15].

In addition to the choice of NIR wavelength, the selection of PPG parameters and the adequate source-detector arrangement (transmittance or reflectance mode) for measuring NIR radiation are also important issues in the studies of noninvasive blood glucose measurements. Yamakoshi et al. [16] studied the geometrical effects of source-detector arrangement (including the source-detector spacing and incident angle of NIR light) to optical absorbance on the fingertip. They concluded the 750–1160 nm range has high signal-to-noise ratio (SNR) in both the transmittance and reflectance modes, while the NIR close to 1550 nm only works better in transmittance mode [16]. Fotouhi-Ghazvini et al. [17] studied both the transmittance and reflectance modes of NIR system for blood glucose measurements. They used three NIR wavelengths, including 940, 1550, and 1650 nm, and found the NIR lights with 1550 and 1650 nm have higher capabilities in the measurement of blood glucose concentrations, compared to the results obtained from 940 nm. The estimation error was larger than $\pm$18 mg/dL in 19 subjects. Gayathri et al. [18] designed a PPG system with single light source to noninvasively measure blood glucose and the estimation error was larger than $\pm$12 mg/dL in 24 subjects with glucose level ranged from 70 to 120 mg/dL.

Together with the previously mentioned issues of wavelength selection and source-detector arrangement, the precise quantification of blood and blood glucose levels underneath the NIR illumination area is also a critical issue. Shokrekhodaei and Quinones [19] summarized that the estimation error of blood glucose using NIR technique could be mainly resulted from two interference components, one is the quantity of blood volume in the NIR illuminated area and the other is the light absorbance by static tissues. For the first issue, the intersubject variation in the sizes of blood vessels should be considered. More blood contained underneath NIR illumination area will result in lower NIR amplitude received by the photodetector. For the second issue, though the effect of water absorption can be reduced by carefully choosing the NIR wavelength with small absorbance coefficient to water, other factors, such as skin color and the components of albumin, globulin, and hemoglobin, can also affect the degree of received NIR intensities [20]. It was less mentioned in previous literatures about how to reduce the variations caused by these two factors in order to improve the estimation accuracy in noninvasive blood glucose measurements.

In this study, we intended to implement a dual-channel system for noninvasive blood glucose estimation. We chose 530 nm green light and 1550 nm NIR light as the dual-light sources, in which the green light is sensitive to hemoglobin

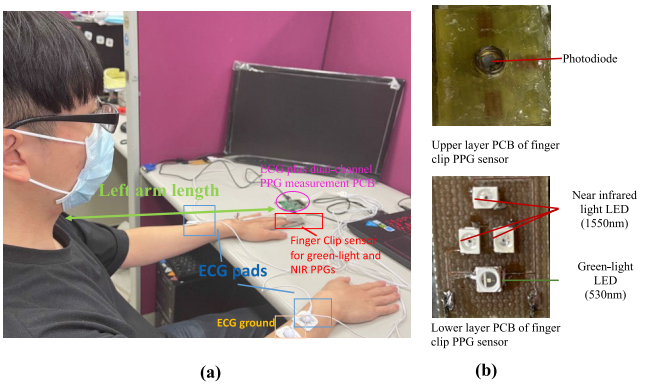

Fig. 1. Experimental setup of our dual-channel PPG and ECG recording. (a) The dual-channel PPG signals were obtained from subject's left index finger, and the ECG signals were recorded from limb lead I. (b) The upper layer and lower layer of the printed circuit boards (PCBs) embedded in the finger-clip probe.

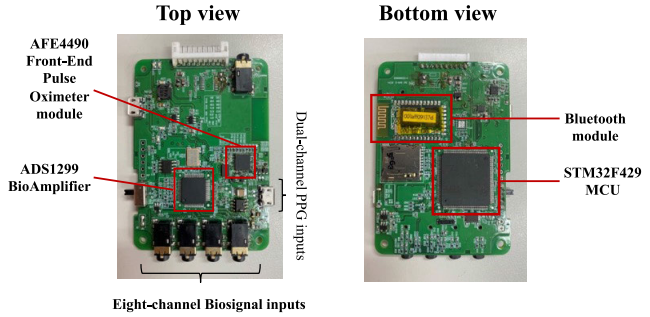

Fig. 2. Eight-channel ECG and dual-channel PPG measurement circuit created by our laboratory. In this study, only one channel of ECG (Limb lead I) and dual-channel PPG signals were recorded. The signals were digitized using an ARM microprocessor and then wirelessly transmitted to a PC.

(deoxyhemoglobin and oxyhemoglobin) and the 1550 nm NIR is sensitive to the glucose concentration. This dual-channel system utilizes infrared light to measure the information of subject's blood glucose, while also using green light to detect the information about blood volume. The optical characteristics of the light sources are different with distinct measured physiological information, so that the additional information provided from the green light can be used to calibrate the blood glucose information obtained from the infrared light, thereby improving the accuracy of blood glucose detection. In this study, we also compared the results of blood glucose estimations from features of single green-light source, single NIR-light source, blood pressure propagation velocity derived from ECG and green/NIR-light PPG, and different feature combinations. The results of this study are expected to further improve the accuracy of noninvasive blood glucose measurement for the benefit of diabetic patients.

II. Materials and Methods

A. ECG and PPG Recording

In our study, we considered the feasibility of dual-channel PPG and blood pressure propagation velocity for blood glucose estimation, which had been mentioned in some previous works of literature [7], [21]. Therefore, we developed a measurement system for acquiring both the dual-channel PPG and ECG data. The dual-channel PPG system included a green light and an NIR light channel, measured through three 1550 nm NIR LEDs (OIS-150-1550p-X-T OSA Opto, OSA Opto Light GmbH, Berlin, Germany) and one 530 nm green-light LED (LT8A23-43-UDC9-TD, LedTech Company, Taipei, Taiwan), measuring in transmittance mode. The three NIR LEDs were connected in parallel with each other and back-to-back connected with the green-light LED in an H-bridge scheme, driven by an analog front-end pulse-oximeter IC (AFE4490, Texas Instruments Inc., Dallas, TX, USA). The ECG signals were amplified using ADS1299 bioamplifier (Texas Instruments Inc., USA). The pulse arrival velocity (PAV) was derived by measuring the pulse arrival time (PAT) between the *R*-wave of each ECG cycle and the systolic point of its corresponding PPG wave. Subject's PAV was obtained from dividing his/her arm length by PAT. Fig. 1 shows the experimental setup of our dual-channel PPG and ECG recording. The dual-channel PPG signals were obtained from the subject's left index finger, while the ECG signals were recorded from limb lead I, with the positive electrode placed on the left wrist, the negative electrode placed on the right wrist, and the ground electrode also placed on the right wrist, just next to the negative ECG lead [see Fig. 1(a)]. The upper layer and lower layer of the printed circuit boards (PCBs) embedded in the finger-clip probe for acquiring dual-channel PPG signals are shown in Fig. 1(b). The lower layer contained three NIR LEDs and one green-light LED, while the upper layer contained one high-speed InGaAs photodiode (MTPD1346D-150, MarkTech Company Ltd., USA) with a spectral sensitivity range of 500–1750 nm. The dual-channel PPG and ECG signals obtained from AFE4490 and ADS1299 were digitized at 500 Hz with 24-bits resolution. The ARM 180 MHz Cortex-M4 microprocessor (32-bit Cortex M4 STM32F411, STMicroelectronics Company) was used to communicate with the AFE4490 and ADS1299 chips through serial peripheral interface (SPI) bus interface at 30 MHz for simultaneously recording of dual-channel PPG and ECG signals (see Fig. 2). The recorded data were wirelessly transmitted (Bluetooth 3.0) to a personal computer for regression analysis using Matlab software (Matlab 2022b, Terasoft Company, USA). The characteristics of the ECG and dual-light PPG instrumentation is listed in Table I.

B. Subjects and Experiment Task

In this study, we recruited 18 healthy subjects (14 males and four females; aged 29.4 ± 7.87 years-old). All subjects were asked to participate in an oral glucose tolerance test (OGTT) [22]. Each subject was instructed to fast (not eat) overnight and then drank a cup of 250 mL glucose solution (containing 75 g glucose dissolved in 250 mL of distilled water). The glucose solution was requested to be consumed within 5 min. Each subject underwent the two times of ECG plus dual-channel PPG measurements, one before they drank the glucose solution and the other 30 min after drinking the glucose solution. Each measurement lasted for three minutes. We used "finger stick blood sugar tests" (accuracy: estimation error within ±15 mg/dL at glucose concentration less than 75 mg/dL and within ±20% at glucose concentration greater or

TABLE I
CHARACTERISTICS OF ECG AND DUAL-LIGHT PPG INSTRUMENTATION

Device	ECG	Green-light PPG	NIR-light PPG
Measurement Location	Limb lead I (ECG+: left wrist ECG- : right wrist Ground: right wrist)	Transmission PPG (Left index finger)	Transmission PPG (Left index finger)
Measured physiological parameters	Electric activity of the heart	Optical measurement of arterial volume (wavelength: 530 nm) is primarily sensitive to hemoglobin and has a low absorption coefficient for blood glucose.	Optical measurement of arterial volume (wavelength: 1550nm) is primarily sensitive to water and glucose concentration and has a low absorption coefficient for hemoglobin.
Sensor for measurement	Electrode Pad	Photodiode	Photodiode
Data recording	ADS1299 EEG Front-End connected with microprocessor through SPI interface	AFE4490 EEG analog Front-End connected with microprocessor through SPI interface	AFE4490 EEG analog Front-End connected with microprocessor through SPI interface
Medium for signal transmission	Electrical wave through the conductivity of the body	Pressure wave through blood vessel	Pressure wave through blood vessel
Wave propagation speed	3×10^8 m/sec	6 m/sec ~ 14 m/sec	6 m/sec ~ 14 m/sec

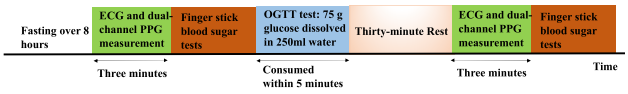

Fig. 3. Experimental protocol of this study; 3-min ECG plus dual-channel PPG measurements were performed before and after OGTT test. Following each ECG plus dual-channel PPG measurement, a finger stick blood sugar test was administered to the subjects as a reference value for subsequent blood sugar regression analysis.

equal to 75 mg/dL; AccuChek Inform II, Roche Diagnostics, USA) to measure the participant's actual blood glucose levels after each measurement. The blood glucose values were used to train our blood glucose regression model. The experimental protocol is shown in Fig. 3.

C. Electrocardiogram (ECG) Signal Processing

To obtain PAVs, the time differences between the R waves of ECG signals and the systolic peaks in the dual-channel PPG signals were detected. We detected the R waves in ECG signals using the Pan–Tompkins algorithm [23]. The subject's ECG signal was first filtered within 5–15 Hz (Bandpass filtering, third-order Butterworth IIR filter) to remove low-frequency drifts and high-frequency noise, and then the signal is differentiated, squared, and integrated using a 150 ms

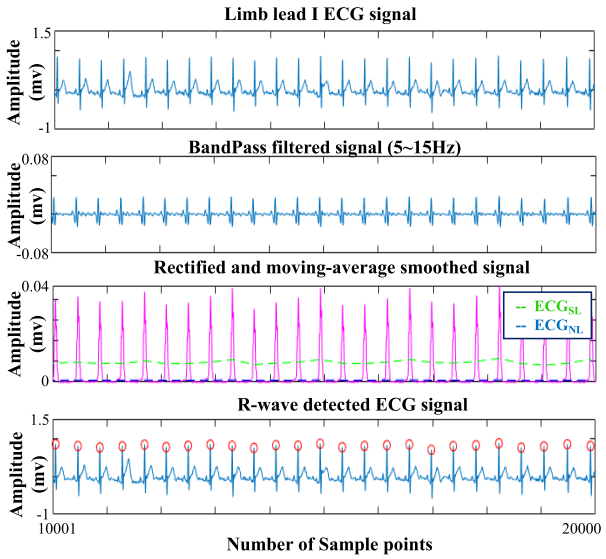

Fig. 4. Signal processing of R wave detection using Pan–Tompkins algorithm. First panel: The measured limb lead I ECG signal. Second panel: The ECG signal filtered within 5–15 Hz. Third panel: The rectified and smoothed signal of the bandpass ECG signal, in which the ECG_{SL} (green dashed line) and the ECG_{NL} (blude dashed line) were the running estimations of the signal and noise levels. Fourth panel: The detected R waves marked by red circles.

moving-average window to obtain an integrated signal. The position of the QRS complex in the ECG was then determined by detecting the peak position in the integrated signal. The signal level, denoted as ECG_{SL}, and the noise level, denoted as ECG_{NL}, were defined to obtain a threshold ECG_{th} for R wave detection, according to (1). The R wave of ECG signal was detected by finding the maximum value within the time window selected by the ECG_{th}. After each R wave being detected, no R wave was detected in the next 200 ms. The ECG_{th} in the running integrated ECG signal was defined using the following equation:

$$ECG_{th} = ECG_{NL} + 0.25(ECG_{SL} - ECG_{NL}) \tag{1}$$

where the ECG_{SL} and the ECG_{NL} were the running estimations of the signal and noise levels in the ECG-integrated signal.

The ECG_{SL} and the ECG_{NL} were automatically updated after detecting a new peak, based on its classification as a signal or noise peak:

$$\begin{cases} ECG_{SL} = 0.125 \cdot Amp_{Peak} + 0.875 \cdot ECG_{SL} \\ \quad \text{(if the Peak is classified as a signal peak)} \\ ECG_{NL} = 0.125 \cdot Amp_{Peak} + 0.875 \cdot ECG_{NL} \\ \quad \text{(if the Peak is classified as a noise peak)} \end{cases} \tag{2}$$

where Amp_{Peak} is the amplitude of a new peak found in the integrated signal. The timing of the R wave was denoted as T_R for the following PAV calculation.

Fig. 4 shows an example of using the Pan–Tompkins algorithm to detect the R waves in a segment of ECG signal. The measured ECG signal was processed with a bandpass filter. Then, the signal was rectified and smoothed using a moving average filter. The ECG_{SL} and ECG_{NL} levels were

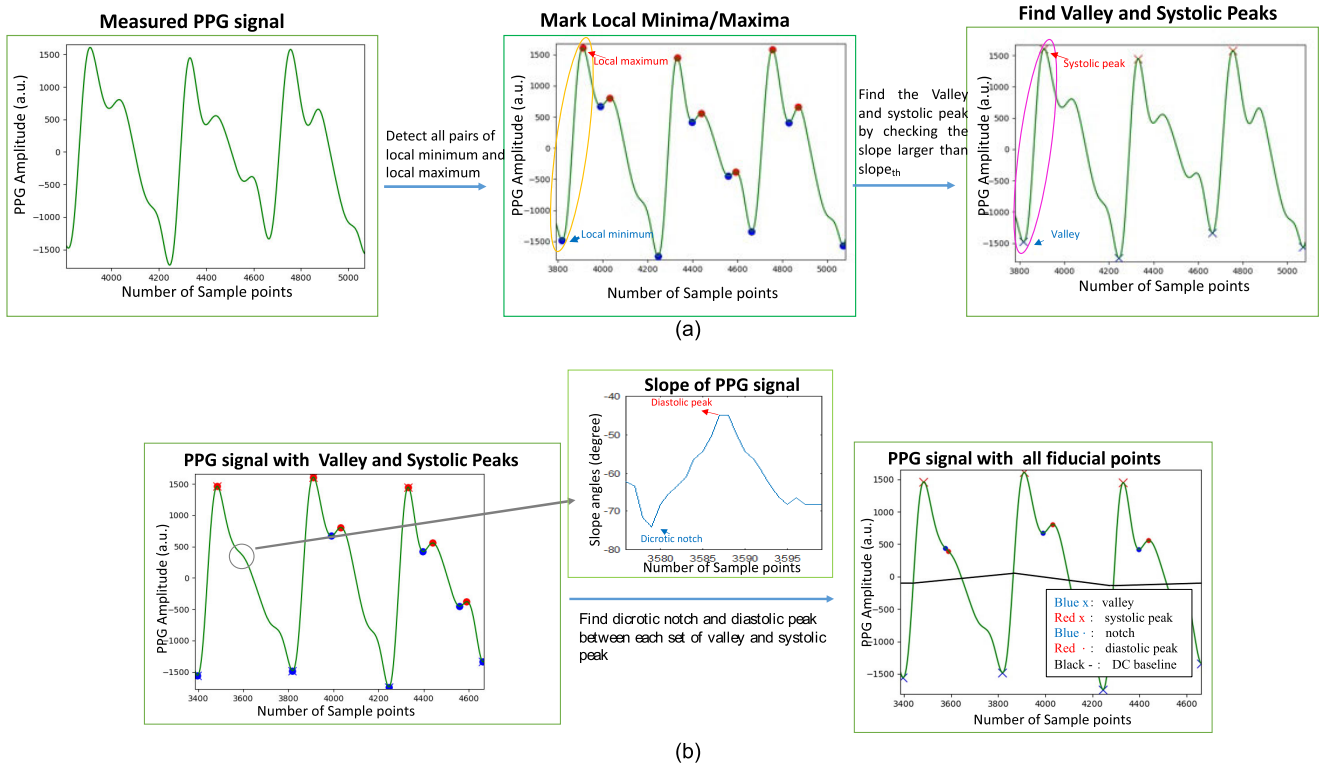

Fig. 5. PPG signal processing for finding fiducial points (valley, systolic peak, dicrotic notch, and diastolic peak). (a) Detection of the valleys and systolic peaks. Left panel: the measure PPG signal, middle panel: the labeling of all local maxima and local minima, and right panel: finding the valleys and systolic peaks with slope exceeding slope_{th}. (b) Detection of the dicrotic notches and diastolic peaks. Left panel: finding the pair of local minimum and local maximum which is closest after the systolic peak by detecting the sign changes of slope values, middle panel: finding the local minimum and local maximum from the slope derivative for the PPG cycle which local minimum and local maximum is not found in previous step, and right panel: labeling the set of local minimum and local maximum after each set of valley and systolic peak as dicrotic notch and diastolic peak.

updated, and the local peaks were selected as the *R* waves of the ECG cycles.

D. Photoplethysmography (PPG) Signal Processing

The dual-channel PPG signals were transmitted to the PC via Bluetooth 3.0. Both channels of the PPG signals were first passed through a 0.5–5 Hz BandPass filter (Bandpass filtering, third-order Butterworth IIR filter) to filter out PPG-unrelated noise, and then the valley, systolic peak, notch amplitude, and diastolic peak of both the PPG signal were detected.

1) Detection of Valley and Systolic Peak Using Mountaineer's Method: Valley and systolic peaks are respectively the lowest and highest points in a PPG cycle. The points of valley and systolic peaks were detected using the following procedure. We first differentiated the PPG signal, and all points where the slope changed from negative to positive were marked as local minima, while all points where the slope changed from positive to negative were marked as local maxima. Due to the variation in the signal, local minimum and local maximum appeared alternately in a PPG cycle. In the PPG signal, the valley and systolic peak appeared as a pair of adjacent local minimum and local maximum, and the slope between each set of local minimum and the local maximum was defined as $\text{slope}_{\text{VtoP}}$. Although there might be more than one set of adjacent local minima and local maxima in the entire PPG cycle, the valley and systolic peak of the PPG must be the set with the largest slope increase in a PPG cycle. Since a person's heart rate does not typically fall below 30 beats per minute in a resting state, we used a window length of two seconds with a sliding window interval of 0.3 s to search for the valley and systolic peak in each time window. We identified the $\text{slope}_{\text{VtoP}}$ with the maximum slope in the time window as $\text{slope}_{\text{max}}$, and defined a slope threshold value, $\text{slope}_{\text{th}} = 0.7 \times \text{slope}_{\text{max}}$, to find the valley and systolic peaks. We then set the local minimum and local maximum of all $\text{slope}_{\text{VtoP}}$s exceeding the slope_{th} in the time window as the valley and systolic peaks. Fig. 5(a) shows one example of the detection process for valley and systolic peaks in a time window. The local maxima and local minima were all labeled, and the sets of local minimum and local maximum with their $\text{slope}_{\text{VtoP}}$s larger than the slope_{th} were chosen as valleys and systolic peaks.

2) Detection of Dicrotic Notch and Diastolic Peak: Since the dicrotic notch marks the end of ventricular systole during a heart contraction, while the diastolic peak is a peak in blood flow as blood flows back into the blood vessels during the relaxation phase of the heart. Therefore, measuring the dicrotic notch and diastolic peak requires identifying a set of local minimums and maximums between the systolic peak and the next valley in a PPG cycle. As shown in Fig. 5(b), the dicrotic notch is the maximum point where the slope changes from negative to positive after the systolic peak, while the diastolic peak is the maximum point where the slope changes from positive to negative after the dicrotic notch and before the next valley. The baseline, marked in black solid line, was calculated

by connecting the mean of amplitude values in adjacent sets of valleys and systolic peaks. The baseline was used to calculate the fluctuations caused by motion or unexpected disturbances. PPG cycles with baseline fluctuations larger than 10% of the amplitude of the systolic peak were excluded from our blood glucose estimations.

The amplitudes of the fiducial points, including valley, systolic peak, dicrotic notch, and diastolic peak, detected above were defined as A_V, A_s, A_N, and A_D, respectively. The time points at which they occurred were defined as T_V, T_s, T_N, and T_D, respectively. We considered the Beer–Lambert law for the amplitudes of the fiducial points which the intensity attenuation was exponentially attenuated with the concentration, the absorption coefficient, and the length of optical path. Therefore, the amplitude features A_V, A_s, A_N, and A_D were the values taking the logarithm of the measured intensities [24]. We defined the amplitude features of the systolic peak, dicrotic notch, and diastolic peak as $\text{Amp}_S = A_s - A_v$ $\text{Amp}_N = A_N - A_V$, and $\text{Amp}_D = A_D - A_V$, respectively. The amplitude features obtained from the three-minute PPG recordings before and after drinking sugar water of OGTT test were separately averaged to eliminate amplitude variation in each feature. These averaged amplitude features were subsequently utilized in the following linear regression analyses for noninvasive blood glucose estimations.

E. Features for Blood Glucose Regression Analysis

This study applied dual-channel PPG for noninvasive blood glucose estimation. The amplitude features of systolic peak, dicrotic notch, and diastolic peak in green-light PPG were denoted as $\text{Amp}_{S\_\text{green}}$, $\text{Amp}_{N\_\text{green}}$ and $\text{Amp}_{D\_\text{green}}$, respectively, and the amplitude features of systolic peak, dicrotic notch, and diastolic peak in NIR-light PPG were denoted $\text{Amp}_{S\_\text{NIR}}$, $\text{Amp}_{N\_\text{NIR}}$ and $\text{Amp}_{D\_\text{NIR}}$, respectively. We also considered the ratios between these amplitude features in green-light and NIR-light PPGs, as well as the pulse arrival velocities (PAVs) obtained from the time differences between ECG R wave and systolic peaks of dual-channel PPG. The ratios of amplitude features were defined as $\text{Ratio}_S = \text{Amp}_{S\_\text{NIR}}/\text{Amp}_{S\_\text{green}}$, $\text{Ratio}_N = \text{Amp}_{N\_\text{NIR}}/\text{Amp}_{N\_\text{green}}$ and $\text{Ratio}_D = \text{Amp}_{D\_\text{NIR}}/\text{Amp}_{D\_\text{green}}$ for the systolic peaks, dicrotic notches and diastolic peaks in NIR and green-light PPGs.

According to [25], the PAV (m/s) was calculated as follows:

$$\text{PAV} = \text{L(meters)}/\text{PAT(seconds)} \tag{3}$$

in which the PAT is the pulse arrival time $\text{PAT} = T_R - T_S$, L is the subject's left arm length, and T_R and T_S are the timing of the R wave in ECG and the timing of the systolic peak in PPG, respectively. Fig. 6 shows the diagram of our PAV measurement in a 2-s time window. We detected the time of ECG R wave (T_R) and the systolic peak time of PPG wave (T_S), and measured the time difference between T_R and T_S to obtain PAT. Then we divided the length of the subject's left arm (L) by PAT to obtain PAV. Fig. 7 displays the ECG and dual-channel PPG signals in a 10-s time window measured by our system. The bottom-left and bottom-right panels show the enlarged plots of the green-light and NIR-light PPG signals, respectively, in which the PPG fiducial points detected by the algorithm described above are shown.

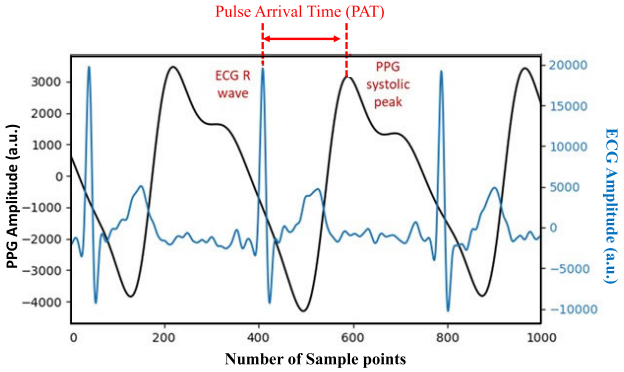

Fig. 6. Diagram shows our PAT measurement. The time difference between the ECG R wave and the systolic peak of its following PPG cycle is defined as PAT. The PAV can be obtained by dividing the subject's arm length by PAT.

TABLE II
LIST OF 11 SIGNAL FEATURES FOR BLOOD GLUCOSE ESTIMATIONS

Feature number	Feature name	Description
1	$\text{Amp}_{S\_\text{green}}$	Systolic peak amplitude of green-light PPG
2	$\text{Amp}_{N\_\text{green}}$	Dicrotic notch amplitude of green-light PPG
3	$\text{Amp}_{D\_\text{green}}$	Diastolic peak amplitude of green-light PPG
4	$\text{Amp}_{S\_\text{NIR}}$	Systolic peak amplitude of near-infrared PPG
5	$\text{Amp}_{N\_\text{NIR}}$	Dicrotic notch amplitude of near-infrared PPG
6	$\text{Amp}_{D\_\text{NIR}}$	Diastolic peak amplitude of near infrared PPG
7	$\text{PAV}_{\text{green}}$	Pulse arrival velocity derived from ECG and green-light PPG
8	PAV_{NIR}	Pulse arrival velocity derived from ECG and NIR-light PPG
9	Ratio_S	Amplitude Ratio of systolic peaks between near-infrared and green-light PPGs
10	Ratio_N	Amplitude Ratio of dicrotic notchs between near-infrared and green-light PPGs
11	Ratio_D	Amplitude Ratio of diastolic peaks between near-infrared and green-light PPGs

We denoted the PAVs of green-light and NIR-light PPGs as $\text{PAV}_{\text{green}}$ and PAV_{NIR}, respectively. The following table lists the 11 features used in this study to achieve the estimation of noninvasive blood glucose values, including the amplitude features of green and NIR-light PPGs, the PAVs of green-light and NIR-light PPGs, and the ratios of amplitude features between green-light and NIR-light PPGs. The list of the features and symbols are shown in Table II.

F. Investigating the Influence of Each Feature in Linear Regression Model Using Partial F-Test

To investigate the influence of each feature, we employed the partial F-test to examine the statistical significance of each feature. The partial F-test first represented the estimated blood glucose value by the 11 features using a linear regression model:

$$Y = \beta_0 + \beta_1 \cdot x_1 + \beta_2 \cdot x_2 + \cdots + \beta_m \cdot x_m + \varepsilon \tag{4}$$

where the $x_1, x_2, \ldots, x_m$ were m features selected from the 11 features in Table II, $\beta_1, \beta_2, \ldots, \beta_m$ are the regression coefficients corresponding to the m features, and the ε represents

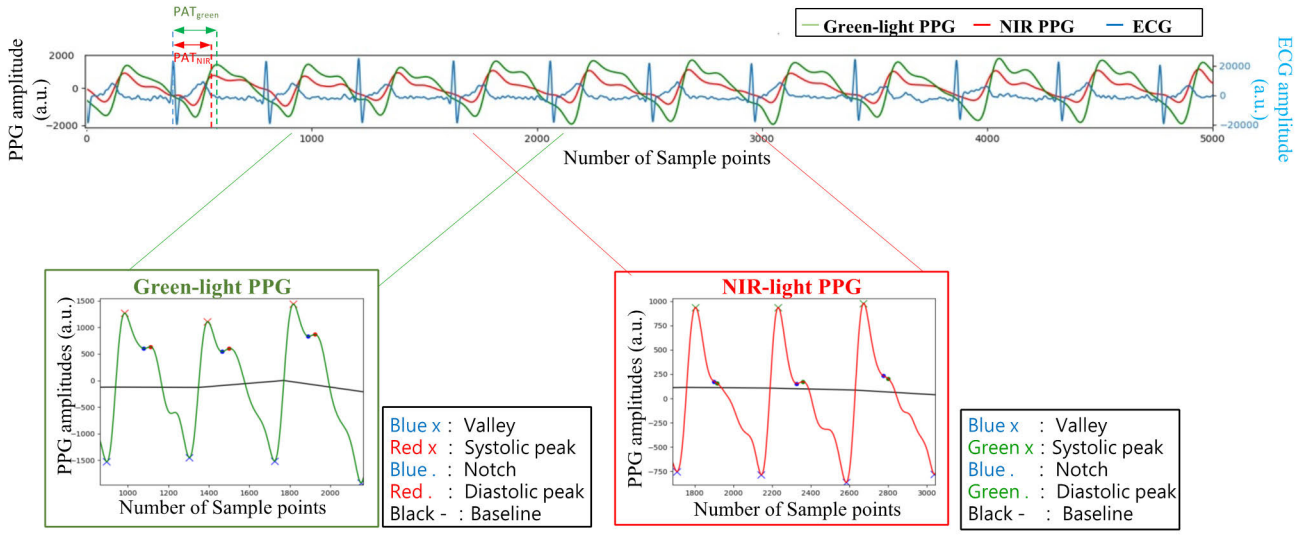

Fig. 7. ECG and dual-channel PPG signals in a ten-second time window. The bottom-left and bottom-right panels show the enlarged plots of the green-light and NIR-light PPG signals, respectively.

the residue between the linear regression output Y and the glucose value measured by the "finger stick blood sugar tests." By excluding a subset of features from these m features and testing whether there is a significant statistical difference between the new reduced model and the full regression model, in order to determine whether the excluded subset of features is significant.

The partial F-test calculates the following F-test statistic [26]:

$$F = ((\mathrm{RSS}_{\mathrm{reduced}} - \mathrm{RSS}_{\mathrm{full}})/p)/(\mathrm{RSS}_{\mathrm{full}}/(n-m)) \quad (5)$$

where $\mathrm{RSS}_{\mathrm{reduced}}$ is the residual sum of squares of the reduced model, $\mathrm{RSS}_{\mathrm{full}}$ is the residual sum of the full model, p is the number of the predictors removed from the full model, n is the total observations in the dataset, and m is the number of coefficients in the full model.

The partial F-test was used to test whether removing a subset of certain features from the full model would result in a significant change in the outcome. In this study, we applied a partial F-test by removing each feature and examining the impact of each feature. The influential features were chosen and combined as predictors for building linear regression models to predict blood glucose levels.

G. Data Analysis and Regression Models

In this study, the ECG plus dual-channel PPG measurement was performed before and after consuming a sugary drink in each subject. The level of blood glucose checked by "finger stick blood sugar tests" was taken as ground truth after each ECG plus dual-channel PPG measurement. Therefore, there were a total of 36 blood glucose measurements and 36 sets of 3-min ECG plus dual-channel PPG measurements from the 18 participants. The blood glucose measurements of these 18 participants were randomly divided into two groups, including 90% of the training data (16 participants) and 10% of the testing data (two participants). The training data was used to build a regression model based on the chosen features and the testing data were used to check the performance of each built regression model. Due to the limited data sample, k-fold cross-validation ($k = 10$) was adopted to reduce the bias of the estimation results. The root-mean-square-error (RMSE) was calculated, and the CEGA was applied to quantify the accuracy of each model in blood glucose estimations. About 16 regression models were tested by choosing distinct feature subsets. The whole experiment procedure was approved by the Ethics Committee of Institutional Review Board (IRB) (Project number: LSIHIRB: 21-003-A2), Landseed International Hospital, Taoyuan, Taiwan, and the study was carried out in accordance with the approved guidelines.

TABLE III
SIGNIFICANCE OF EACH FEATURE EXAMINED USING PARTIAL F-TEST

Item categories	Feature name	Partial F-test		
		t-test value	F-test value	p-value
Amplitude features of green-light PPG	$\mathrm{Amp_{S\_green}}$	0.06114	3.74E-03	9.51E-01
	$\mathrm{Amp_{N\_green}}$	1.2567	1.58E+00	2.09E-01
	$\mathrm{Amp_{D\_green}}$	-7.2736	5.29E+01	7.94E-13**
Amplitude features of NIR-light PPG	$\mathrm{Amp_{S\_NIR}}$	2.6754	7.16E+00	7.61E-03**
	$\mathrm{Amp_{N\_NIR}}$	1.0332	1.07E+00	3.02E-01
	$\mathrm{Amp_{D\_NIR}}$	4.1219	1.70E+01	4.13E-05**
Pulse-wave velocities	$\mathrm{PAV_{green}}$	5.5906	3.13E+01	3.05E-08**
	$\mathrm{PAV_{NIR}}$	-4.6866	2.20E+01	3.23E-06**
Ratio of amplitude features	$\mathrm{Ratio_S}$	8.66	7.50E+01	2.34E-17**
	$\mathrm{Ratio_N}$	2.9943	8.97E+00	2.14E-05**
	$\mathrm{Ratio_D}$	-9.1752	8.42E+01	3.33E-19**

Remark: ** $p < 0.01$

III. RESULTS

We used partial F-test to determine the significance of each feature by testing the statistical significance of removing each feature compared to the full-feature model. Table III lists the results of the partial F-test in examining the 11 features. The t-test value, F-value, and

p-value of each feature in the partial F-test are shown. We recombined these 11 features into 16 different combinations based on the characteristics of each feature. The combinations included $\text{Amp}_{S\_\text{green}}$, $\text{Amp}_{D\_\text{green}}$, $\text{Amp}_{S\_\text{green}}+\text{Amp}_{N\_\text{green}}+\text{Amp}_{D\_\text{green}}$, $\text{Amp}_{s\_\text{NIR}}$, $\text{Amp}_{D\_\text{NIR}}$, $\text{Amp}_{S\_\text{NIR}}+\text{Amp}_{N\_\text{NIR}}+\text{Amp}_{D\_\text{NIR}}$, $\text{PAV}_{\text{green}}$, PAV_{NIR}, $\text{PAV}_{\text{green}}+\text{PAV}_{\text{NIR}}$ Ratio_S, Ratio_D, $\text{Ratio}_S + \text{Ratio}_N + \text{Ratio}_D$, $\text{PAV}_{\text{green}} + PAV_{\text{NIR}} + \text{Ratio}_S + \text{Ratio}_N + \text{Ratio}_D$, $\text{Amp}_{D\_\text{green}} + \text{Amp}_{D\_\text{NIR}} + \text{PAV}_{\text{green}} + \text{PAV}_{\text{NIR}} + \text{Ratio}_S + \text{Ratio}_N + \text{Ratio}_D$, $\text{Amp}_{S\_\text{green}} + \text{Amp}_{S\_\text{NIR}} + \text{Amp}_{D\_\text{green}} + \text{Amp}_{D\_\text{NIR}} + \text{PAV}_{\text{green}} + \text{PAV}_{\text{NIR}} + \text{Ratio}_S + \text{Ratio}_N + \text{Ratio}_D$, and all features. We categorized the 16 feature combinations into four groups, including the amplitude features of green-light PPG, the amplitude features of NIR-light PPG, the PAVs, and the amplitude ratios between NIR-light and green-light PPGs. In the amplitude features of green-light and NIR-light PPGs, we tested the amplitudes of fiducial points, i.e., the systolic peaks, dicrotic notches, and diastolic peaks, and found only the amplitude of diastolic peak in green-light PPG and the amplitudes of the systolic and diastolic peaks in NIR-light PPG were significantly meaningful. Regarding PAVs, both the PAVs for green-light and NIR-light PPG were crucial factors in determining blood glucose levels. Furthermore, it is worth noting that the amplitude ratios of the three fiducial points were all important factors in the estimation of blood glucose levels.

To examine the effectiveness of these features in blood glucose estimation, we have considered different combinations of these features and explored their accuracies in blood glucose estimations using a linear regression model. In Fig. 8, the RMSE of the estimated blood glucose levels obtained for different feature combinations is shown. For the amplitude features of green-light PPG, the RMSE values (mean ± std.) of estimated blood glucose levels were 15.87 ± 6.60, 14.06 ± 6.47, and 14.77 ± 6.54 mg/dL using the regression models predicted by $\text{Amp}_{S\_\text{green}}$, $\text{Amp}_{D\_\text{green}}$ and the combined feature ($\text{Amp}_{S\_\text{green}}+ \text{Amp}_{N\_\text{green}}+ \text{Amp}_{D\_\text{green}}$), respectively. For the amplitude features of NIR-light PPG, the RMSE values (mean ± std.) of estimated blood glucose levels were 9.80 ± 3.82, 9.06 ± 3.52, and 10.10 ± 3.45 mg/dL using the regression models predicted by $\text{Amp}_{S\_\text{NIR}}$, $\text{Amp}_{D\_\text{NIR}}$ and the combined feature ($\text{Amp}_{S\_\text{NIR}}+ \text{Amp}_{N\_\text{NIR}} + \text{Amp}_{D\_\text{NIR}}$), respectively. For the features of PAVs, the RMSE values (mean ± std.) of estimated blood glucose levels were 11.20 ± 4.75, 10.44 ± 4.12, and 11.36 ± 4.87 mg/dL using the regression models predicted by $\text{PAV}_{\text{green}}$, PAV_{NIR} and the combined feature ($\text{PAV}_{\text{green}} + \text{PAV}_{\text{NIR}}$), respectively. For the features of the amplitude ratios, the amplitude ratios of NIR-light PPG and green-light PPG at different fiducial points were combined to build linear regression models for estimation of blood glucose levels. The RMSE values (mean ± std.) of estimated blood glucose levels were 8.30 ± 3.17, 9.09 ± 3.54, and 7.85 ± 3.31 mg/dL using the regression models predicted by Ratio_s, Ratio_D and the combined feature ($\text{Ratio}_s + \text{Ratio}_N + \text{Ratio}_D$), respectively. The bars from numbered 13–16 tried to test the effectiveness of different feature combinations. The feature combination #13 was the feature combination of ($\text{PAV}_{\text{green}} + \text{PAV}_{\text{NIR}} + \text{Ratio}_s + \text{Ratio}_N + \text{Ratio}_D$), and the RMSE value (mean ± std.) was 7.46 ± 2.43 mg/dL. The feature combination #14 was the feature combination of ($\text{Amp}_{D\_\text{green}} + \text{Amp}_{D\_\text{NIR}} + \text{PAV}_{\text{green}} + \text{PAV}_{\text{NIR}} + \text{Ratio}_s + \text{Ratio}_N + \text{Ratio}_D$), and the RMSE value (mean ± std.) was 8.26 ± 2.56 mg/dL. The feature combination #15 was the feature combination of ($\text{Amp}_{S\_\text{green}} + \text{Amp}_{S\_\text{NIR}} + \text{Amp}_{D\_\text{green}} + \text{Amp}_{D\_\text{NIR}} + \text{PAV}_{\text{green}} + \text{PAV}_{\text{NIR}} + \text{Ratio}_s + \text{Ratio}_N + \text{Ratio}_D$), and the RMSE value (mean ± std.) was 9.11 ± 2.52 mg/dL. The feature combination #16 was the feature combination of all features, and the RMSE value (mean ± std.) was 9.16 ± 2.72 mg/dL.

Fig. 9 shows the performances different feature combinations on CEGA in our K-fold cross-validations. The feature combinations were categorized into five categories, including amplitude features of green-light PPG, amplitude features of NIR-light PPG, PAVs, amplitude ratios, and other combinations. The use of features from green-light PPG resulted in higher RMSEs, compared to the results obtained from other feature combinations. This observation is consistent with previous literatures reporting that the NIR light near 1550 nm has good absorption and sensitivity coefficients for blood glucose [27]. Comparing the RMSE of the amplitude features from green-light PPG with the RMSE of amplitude features from infrared PPG, the comparison between the averages of RMSE in the green-light PPG group and the NIR-light PPG group was 14.90 ± 6.54 versus 9.65 ± 3.60 mg/dL, indicating that NIR-light PPG has an advantage over green-light PPG in blood glucose estimation. In addition, although PAV features are statistically significant in our partial F-test (see Table III), the use of PAV did not exhibit superior performance in blood glucose estimation and its RMSE was only lower than those results in the green-light PPG group. Therefore, the PAV features may need to be combined with other PPG features to achieve better performance in blood glucose estimations. It is noteworthy that the amplitude ratio group exhibited better estimation results and lower RMSE, compared to the results of green-light PPG, NIR-light PPG, and PAV feature groups. The benefit of using amplitude ratio might be attributed to its advantage of combining the characteristics of NIR-light PPG in blood glucose estimation and the green- light PPG in blood volume detection, resulting in more accurate results by utilizing the information from two different sources.

Fig. 9(a) shows the blood glucose estimation results using green-light PPG features. The blood glucose levels predicted by the features of $\text{Amp}_{S\_\text{green}}$, $\text{Amp}_{D\_\text{green}}$, and ($\text{Amp}_{S\_\text{green}} + \text{Amp}_{N\_\text{green}} + \text{Amp}_{D\_\text{green}}$) were displayed in black, red, and blue color dots, with 82.65%, 83.67%, and 83.07% falling in Zone A, respectively. Fig. 9(b) shows the blood glucose results obtained from using NIR-light PPG features. The results are displayed on a Clarke error grid, and the blood glucose levels estimated by $\text{Amp}_{S\_\text{NIR}}$, $\text{Amp}_{D\_\text{NIR}}$, and $\text{Amp}_{S\_\text{NIR}} + \text{Amp}_{N\_\text{NIR}} + \text{Amp}_{D\_\text{NIR}}$ are represented by black, red, and blue dots with 96.33%, 95.8%, and 95.45% falling in Zone A, respectively. In Fig. 9(c), the blood glucose estimation results obtained from $\text{PAV}_{\text{green}}$, PAV_{NIR}, and ($\text{PAV}_{\text{green}} + \text{PAV}_{\text{NIR}}$) are represented by black, red, and blue dots, respectively, and their proportions of results falling in

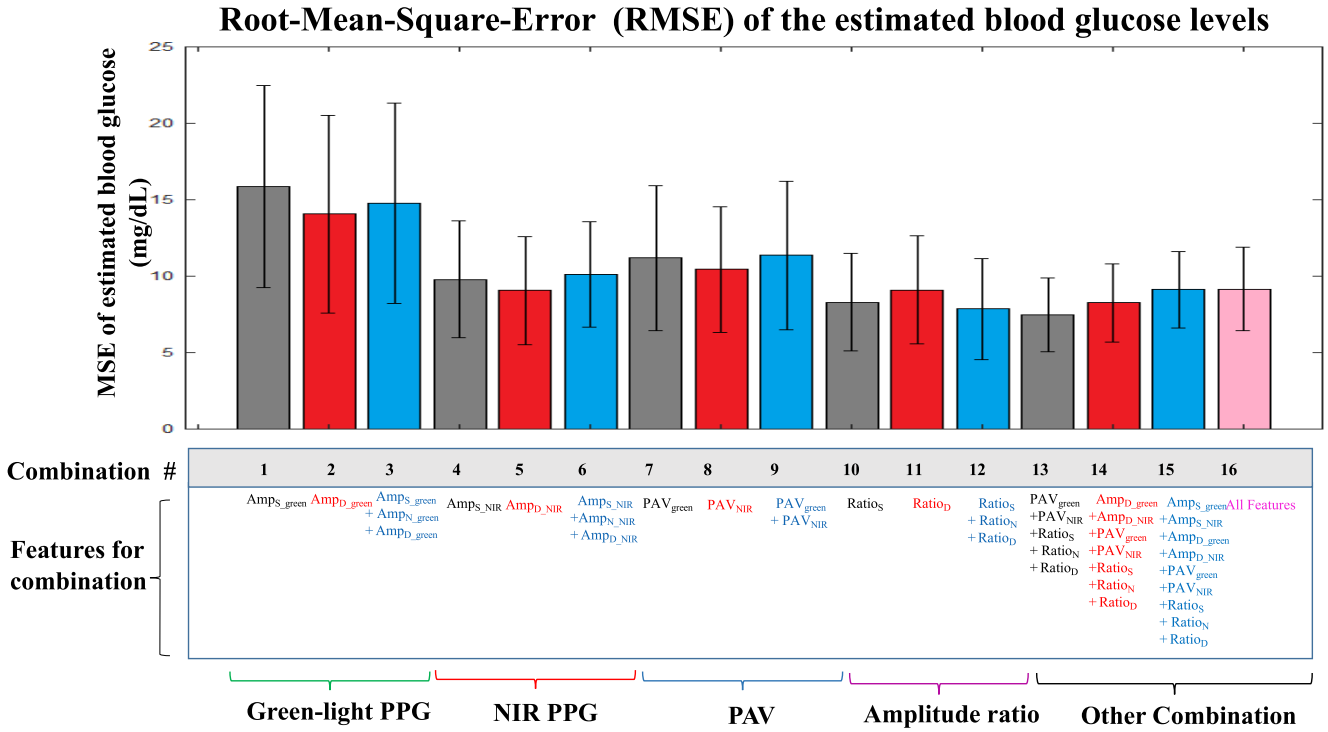

Fig. 8. Root-mean-square-error (RMSE) of the estimated blood glucose levels obtained for different feature combinations. The upper panel shows the RMSE for each feature combination. The lower panel displays the features used for each feature combination.

Zone A are 85.93%, 84.62%, and 82.90%, respectively. In Fig. 9(d), the blood glucose estimation results obtained from the amplitude ratio features are tested. The results from Ratio_S, Ratio_D, and $(\text{Ratio}_S + \text{Ratio}_N + \text{Ratio}_D)$ are represented by black, red, and blue dots, respectively, and their proportions of results falling in Zone A are 100%, 96.45%, and 97.41%, respectively. In Fig. 9(e), we attempted to combine different features, with four feature combinations as follows: PAVs plus amplitude ratios, amplitude of diastolic peaks plus PAV and amplitude ratios, amplitudes of systolic and diastolic peaks plus PAVs and amplitude ratios, and all features. These feature combinations correspond to feature combinations #13–#16 in Fig. 8. The blood glucose estimation values obtained from these feature combinations were displayed in black, red, blue, and pink color dots, with proportions of results falling in Zone A of 100%, 96.41%, 97.92%, and 94.85%, respectively. From Table III and Fig. 9(e), it can be observed that the feature combinations #13–#16 all used the PAV plus amplitude ratio features and achieved lower estimation errors than feature combinations #1–#12 (8.50 ± 2.56 mg/dL versus 10.99 ± 4.51 mg/dL). Especially, feature combination #13 had a CEGA analysis with proportion of 100% falling in Zone A. This may be because the amplitude ratio already contained the feature information of both green-light PPG and NIR-light PPG, and combining it with PAV information covered the characteristics of green-light PPG, NIR-light PPG, and PAV, thus providing the best estimation results.

IV. Discussion

In this study, we developed a noninvasive blood glucose estimation system that combines dual-channel PPGs and PAV. The system combined the advantages of green light in blood flow detection, the high absorption coefficient of infrared light in blood glucose detection, and the contribution of PAV in blood glucose detection from previous literatures [28]. To the best of our knowledge, this is the first noninvasive blood glucose detection system that combines green-light and NIR-light PPGs, as well as PAV measurement. The dual-channel PPGs in this study uses one green light source that is irrelevant to blood glucose measurement [29], and another NIR light source that is sensitive to blood glucose concentration [30]. Considering the Beer–Lambert law, which states that the attenuation of a light source can vary based on the length of the optical path and the concentration of blood glucose [31], using only a NIR light source for blood glucose detection can reveal the relationship between blood glucose and infrared light intensity but cannot account for the optical path length within the irradiation area. Therefore, we utilized the transmissive dual-channel PPG measurements where the optical length of the green-light PPG was approximately equal to the optical length of the NIR-light PPG [32]. The amplitude ratio of the NIR-light PPG and the green-light PPG was used to calibrate the variant caused by optical length in the amplitude of the NIR-light PPG. The research results (as shown in Table III) demonstrate that the RMSE of using amplitude ratio (feature combinations #10–#12) is lower than that of using only NIR features (feature combinations #4–#6) (8.42 ± 3.34 mg/dL versus 9.65 ± 3.60 mg/dL). The CEGA analysis also revealed that the blood glucose estimations obtained by using amplitude ratios were superior to those obtained by using only NIR-light PPG features [see Fig. 9(b) and (d)].

This study innovatively utilizes 530 nm green visible light and 1550 nm near-infrared light for noninvasive blood glucose research. The 530 nm green visible light, located in the visible range, is relevant to the concentration of hemoglobin and responds to the blood volume underlying the illumination area,

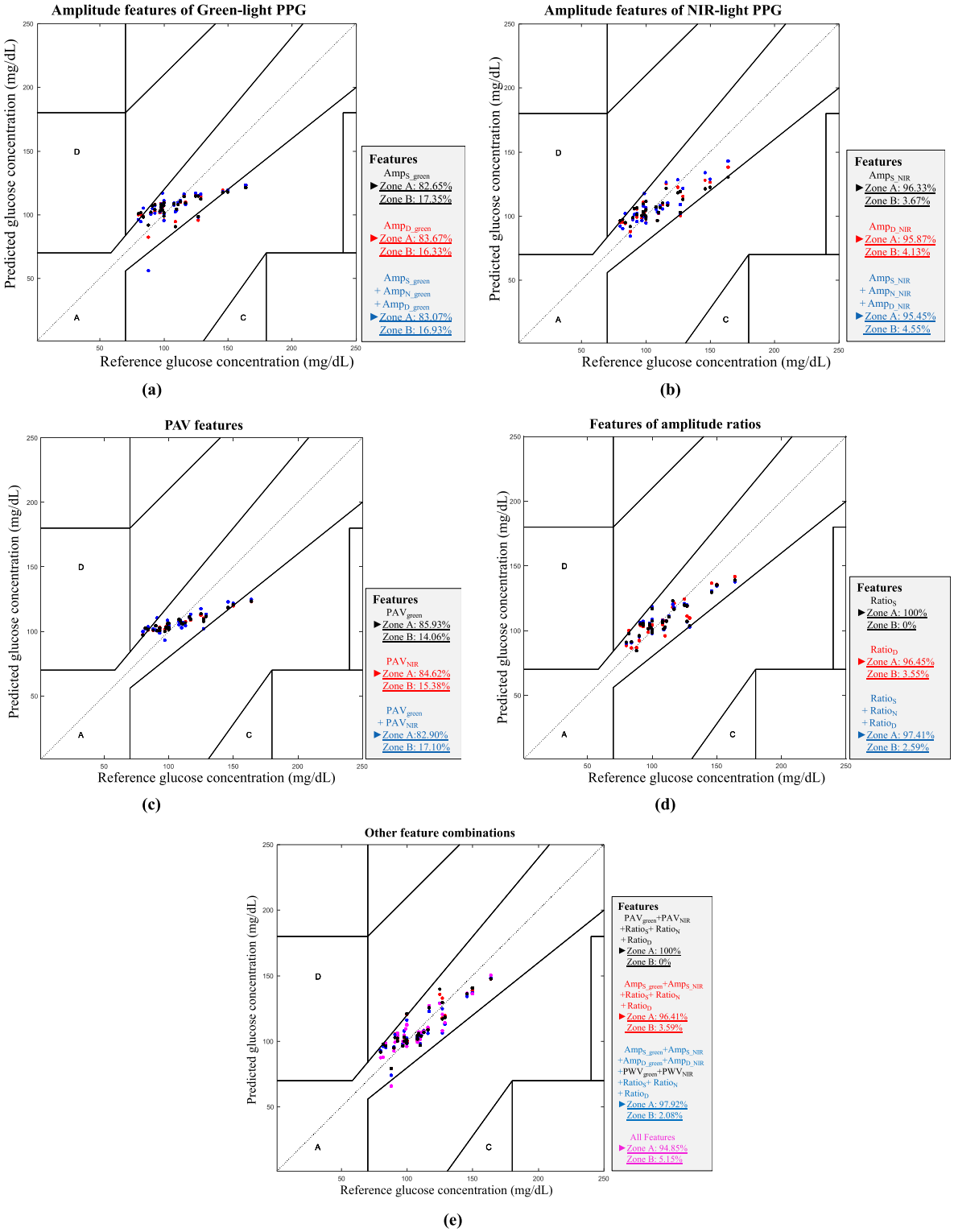

Fig. 9. Clarke Error Grid Analysis (CEGA) of the blood glucose levels predicted by different features combinations. The colored dots marked the predicted blood glucose values in the *k*-fold cross-validations. (a) Predicted blood glucose levels using amplitude features of green-light PPG. (b) Predicted blood glucose levels using amplitude features of NIR-light PPG. (c) Predicted blood glucose levels using PAV features. (d) Predicted blood glucose levels using the features of amplitude ratios. (e) Predicted blood glucose levels using different feature combinations selected from amplitude features, PAV features, and amplitude ratios of dual-light PPGs.

while the 1550 nm near-infrared light, located in the invisible range, is sensitive to blood glucose concentration but not to hemoglobin. With the distinct information provided by the two light sources, the dual-channel PPG system enables the combination of blood volume and blood glucose information for better blood glucose estimation. Several multiwavelength PPG studies had been conducted for blood glucose estimations. Zhang et al. [9] used a mobile phone camera to capture images of red, green, and blue components, and extracted PPG signals through grayscale changes in pixels over time. However,

in their study, only the red image component could capture the PPG signals, while the green and blue image components did not provide clear PPG signals for blood glucose analyses. The image components captured from camera were not integrated for blood glucose estimations. Yen et al. [33] used 660 and 830 nm, plus a bioelectric impedance meter, to estimate subjects' blood glucose levels. However, the 660 and 830 nm light sources could easily be confused with the concentration of oxyhemoglobin and deoxyhemoglobin and cause variations in blood glucose estimations. Castro-Pimentel et al. [34] built a three-wavelength (525, 660, and 940 nm) system for blood glucose estimation. The three-wavelength signals were analyzed using SVMs and had 95.38% of predicted blood glucose values falling within the Zone A in CEGA. However, in most current studies of blood glucose estimation, PPG measurements were conducted using light wavelengths close to or below 1000 nm, which have high absorption coefficients for hemoglobin. This leads to inevitable variations caused by changes in hemoglobin concentration. Therefore, in these systems using wavelengths close to 1000 nm, it could be challenging to reduce the interference caused by changes of hemoglobin concentration. In our system, we carefully chose wavelengths of dual-channel light sources for blood glucose estimation. We used 530 nm green light, which is irrelevant to blood glucose, and 1550 nm near-infrared light that is insensitive to hemoglobin but has a high absorption coefficient for blood glucose. The simultaneous measurement of NIR-light PPG and green-light PPG can help correct interindividual differences in blood volume under the illuminated area on the fingertips, resulting in more accurate blood glucose estimation.

In previous works of literature, several research teams have explored the feasibility of using PWV to detect subjects' blood glucose levels [7], [35]. Although some papers have mentioned the importance of PWV in detecting diabetes, most of the research on PWV and diabetes still focuses on measuring vascular stiffness and cardiovascular diseases [36], [37], [38]. Few papers have directly examined the correlation between PWV and actual blood glucose levels. In our study, we used the partial F-test to investigate the significance of PAV and found the PAV was a significant factor in estimating blood glucose levels. However, when we subsequently applied PAV to establish a linear regression model (feature combinations 7–9), the linear regression model built from PAV did not present superior results [see Figs. 8 and 9(c)]. Nevertheless, the accuracies of blood glucose detections were improved when we combined the PAV features with other amplitude features (see feature combinations #13–#16 in Fig. 8). Hence, it would be interesting to exclude the influence of age [35] and vascular stiffness [39], and investigate whether PAV is a factor solely related to the changes of blood glucose levels. To clarify the influence of blood glucose levels on PAV, only normal subjects were recruited in this study, and OGTT was used as the factor to control the subject's blood glucose levels. Li et al. [40] explained that changes in blood viscosity can cause changes in PAV. Although using the partial F-test can roughly show the impact of PAV on blood glucose changes, other PPG feature parameters are still needed to accurately estimate blood glucose levels. This might be the reason why adding PAV to other PPG features can improve the accuracy of blood glucose estimations [see Figs. 8 and 9(e)].

The PAV was derived from the PAT by measuring the time difference between the R wave of ECG and the PPG systolic peak. It consists of the preejection period (PEP), which represents the time between electrical activation of the ventricles and the pulse wave after the aortic valve opening, and the pulse transit time (PTT), which is the transmission time of the blood pressure wave from the heart to the peripheral limb. Some studies on blood pressure estimation considered PEP as a variable unrelated to the propagation time of the blood pressure wave, which may introduce uncertainty in blood pressure measurements. However, according to the study by Synowski et al. [41], PEP reflects information about blood glucose, as increased blood glucose levels lead to a shortened PEP duration. Wang et al. [42] found a negative correlation between blood glucose levels and the mean standard deviation of the 5-min R–R interval (SDNN). Since PEP is related to sympathetic nervous system activity, the shortened PEP duration may be associated with increased sympathetic activity caused by elevated blood glucose levels. Additionally, regarding PTT, Lee et al. [43] observed a significant increase in brachial ankle pulse wave velocity (PWV) in healthy subjects after undergoing OGTT, indicating that PTT shortens with increased blood glucose levels. Therefore, compared to other PPG studies that solely rely on PTT [44], [45], using PAT obtained from ECG and PPG provides additional information reflecting glucose-related changes, including PEP and PTT. Therefore, in our study, we used PAT as one of the parameters for glucose estimation instead of PTT. This may also explain why PAT achieved statistical significance in our partial F-test. Nevertheless, in the linear regression results using $\text{PAV}_{\text{green}}$ and PAV_{NIR} alone [see Fig. 9(c)], the proportions of estimated blood glucose values falling in Zone A were only 85.93% and 82.90%, respectively, which were lower than the results of using NIR-light PPG alone [see Fig. 9(b)] and the ratios of amplitude features [see Fig. 9(d)]. Although PAV can provide additional information compared to amplitude features in blood glucose estimation, its accuracy was still low due to several unknown factors. More research is needed in the future to enhance the accuracy of PAV in blood glucose estimation.

V. Conclusion

The article investigated the feasibility of using dual-channel PPG combined with PAV for noninvasive blood glucose estimation. We innovatively utilized the advantages of 530 nm green-light PPG in blood volume detection and the 1550 nm NIR-light PPG in glucose concentration detection, and combined these two PPG channels for noninvasive blood glucose estimation. We also explored whether the PAV and amplitude ratio feature between infrared and green PPG have significant implications for blood glucose estimation. In this article, instead of studying patients with diabetes as done in previous studies, we primarily focused on measuring young and healthy subjects. The purpose was to eliminate the influence of factors such as vascular hardening and cardiovascular diseases, particularly as PAV has been linked to arterial stiffness in many studies. Therefore, we conducted OGTT experiments

to manipulate the blood glucose levels of normal young individuals, which allowed us to eliminate uncertainties caused by age-related and cardiovascular disease-related factors, and more accurately assessed the importance of these blood glucose estimation factors in relation to blood glucose variations.

The salient features proposed in this article are as follows: 1) using dual-channel green and infrared PPG for blood glucose estimation; 2) using dual-channel PPG combined with PAV for blood glucose estimation; 3) innovatively utilizing the amplitude ratio between dual-channel PPG as a parameter for blood glucose estimation; 4) using dual-channel PPG combined with PAV as parameters for blood glucose estimation; and 5) testing the importance of each parameter for blood glucose estimation using partial F-test. This article presents a comprehensive analysis of the impact of different parameters on blood glucose estimation, as well as their results in terms of CEGA and RMSE. In our study, using dual-channel PPG combined with PAV, the estimation results fallen within Zone A in CEGA with a 100% success rate, and the RMSE is 7.46 ± 2.43 mg/dL.

REFERENCES

[1] K. Kaul, J. M. Tarr, S. I. Ahmad, E. M. Kohner, and R. Chibber, "Introduction to diabetes mellitus," in *Diabetes: Old Disease, a New Insight*. New York, NY, USA: Springer, 2013, pp. 1–11.

[2] M. A. Arnold, "Non-invasive glucose monitoring," *Current Opinion Biotechnol.*, vol. 7, no. 1, pp. 46–49, 1996.

[3] H. M. Heise, A. Bittner, and R. Marbach, "Near-infrared reflectance spectroscopy for noninvasive monitoring of metabolites," *cclm*, vol. 38, no. 2, pp. 137–145, Feb. 2000.

[4] A. M. Enejder et al., "Blood analysis by Raman spectroscopy," *Opt. Lett.*, vol. 27, no. 22, pp. 2004–2006, 2002.

[5] A. M. Enejder et al., "Raman spectroscopy for noninvasive glucose measurements," *J. Biomed. Opt.*, vol. 10, no. 3, pp. 031114-1–031114-9, May/Jun. 2005.

[6] B. R. Jean, E. C. Green, and M. J. McClung, "A microwave frequency sensor for non-invasive blood-glucose measurement," in *Proc. IEEE Sensors Appl. Symp.*, Feb. 2008, pp. 4–7.

[7] D. Kulik, D. Zubko, A. Markvart, L. Liokumovich, and N. Ushakov, "Non-invasive blood glucose estimation using two multiplexed fiber-optic Fabry–Pérot interferometric sensors and pulse wave signal features analysis," in *Proc. Int. Youth Conf. Electron., Telecommun. Inf. Technol. (YETI)*. St. Petersburg, Russia: Springer, Jan. 2022, pp. 449–456.

[8] R. Garcia-Carretero, L. Vigil-Medina, I. Mora-Jimenez, C. Soguero-Ruiz, O. Barquero-Perez, and J. Ramos-Lopez, "Use of a K-nearest neighbors model to predict the development of type 2 diabetes within 2 years in an obese, hypertensive population," *Med. Biol. Eng. Comput.*, vol. 58, no. 5, pp. 991–1002, May 2020.

[9] G. Zhang et al., "A noninvasive blood glucose monitoring system based on smartphone PPG signal processing and machine learning," *IEEE Trans. Ind. Informat.*, vol. 16, no. 11, pp. 7209–7218, Nov. 2020.

[10] S. Habbu, M. Dale, and R. Ghongade, "Estimation of blood glucose by non-invasive method using photoplethysmography," *Sādhanā*, vol. 44, no. 6, p. 135, Jun. 2019.

[11] L. A. Philip, K. Rajasekaran, and E. S. J. Jothi, "Continous monitoring of blood glucose using photophlythesmograph signal," in *Proc. Int. Conf. Innov. Electr., Electron., Instrum. Media Technol. (ICEEIMT)*, Feb. 2017, pp. 187–191.

[12] M. A. Al-dhaheri, N.-E. Mekkakia-Maaza, H. Mouhadjer, and A. Lakhdari, "Noninvasive blood glucose monitoring system based on near-infrared method," *Int. J. Electr. Comput. Eng. (IJECE)*, vol. 10, no. 2, p. 1736, Apr. 2020.

[13] T. T. Islam, M. S. Ahmed, M. Hassanuzzaman, S. A. B. Amir, and T. Rahman, "Blood glucose level regression for smartphone PPG signals using machine learning," *Appl. Sci.*, vol. 11, no. 2, p. 618, Jan. 2021.

[14] J. Yadav, A. Rani, V. Singh, and B. M. Murari, "Prospects and limitations of non-invasive blood glucose monitoring using near-infrared spectroscopy," *Biomed. Signal Process. Control*, vol. 18, pp. 214–227, Apr. 2015.

[15] T. Vahlsing, S. Delbeck, S. Leonhardt, and H. M. Heise, "Noninvasive monitoring of blood glucose using color-coded photoplethysmographic images of the illuminated fingertip within the visible and near-infrared range: Opportunities and questions," *J. Diabetes Sci. Technol.*, vol. 12, no. 6, pp. 1169–1177, Nov. 2018.

[16] Y. Yamakoshi et al., "Side-scattered finger-photoplethysmography: Experimental investigations toward practical noninvasive measurement of blood glucose," *J. Biomed. Opt.*, vol. 22, no. 6, Jun. 2017, Art. no. 067001.

[17] F. Fotouhi-Ghazvini, B. Javid, and F. Zakeri, "Noninvasive optical diagnostic techniques for mobile blood glucose and bilirubin monitoring," *J. Med. Signals Sensors*, vol. 8, no. 3, p. 125, 2018.

[18] B. Gayathri, K. Sruthi, and K. A. U. Menon, "Non-invasive blood glucose monitoring using near infrared spectroscopy," in *Proc. Int. Conf. Commun. Signal Process. (ICCSP)*, Apr. 2017, pp. 1139–1142.

[19] M. Shokrekhodaei and S. Quinones, "Review of non-invasive glucose sensing techniques: Optical, electrical and breath acetone," *Sensors*, vol. 20, no. 5, p. 1251, Feb. 2020.

[20] J. T. Kuenstner, K. H. Norris, and W. F. McCarthy, "Measurement of hemoglobin in unlysed blood by near-infrared spectroscopy," *Appl. Spectrosc.*, vol. 48, no. 4, pp. 484–488, Apr. 1994.

[21] K. Aso et al., "Brachial-ankle pulse wave velocity is useful for evaluation of complications in type 2 diabetic patients," *Hypertension Res.*, vol. 26, no. 10, pp. 807–813, 2003.

[22] E. Bartoli, G. P. Fra, and G. P. C. Schianca, "The oral glucose tolerance test (OGTT) revisited," *Eur. J. Internal Med.*, vol. 22, no. 1, pp. 8–12, Feb. 2011.

[23] H. Sedghamiz. (2014). *MATLAB Implementation of Pan Tompkins ECG QRS Detector*. File Exchange Site of MathWorks. [Online]. Available: https://de.mathworks.com/matlabcentral/fileexchange/45840-complete-pan-tompkins-implementation-ecg-qrs-detector

[24] L. Kocsis, P. Herman, and A. Eke, "The modified Beer–Lambert law revisited," *Phys. Med. Biol.*, vol. 51, no. 5, pp. N91–N98, Mar. 2006.

[25] J. I. Davies and A. D. Struthers, "Pulse wave analysis and pulse wave velocity: A critical review of their strengths and weaknesses," *J. Hypertension*, vol. 21, no. 3, pp. 463–472, Mar. 2003.

[26] M. Jamshidian, R. I. Jennrich, and W. Liu, "A study of partial F tests for multiple linear regression models," *Comput. Statist. Data Anal.*, vol. 51, no. 12, pp. 6269–6284, Aug. 2007.

[27] J. Dai, Z. Ji, Y. Du, and S. Chen, "In vivo noninvasive blood glucose detection using near-infrared spectrum based on the PSO-2ANN model," *Technol. Health Care*, vol. 26, pp. 229–239, May 2018.

[28] P.-C. Hsu, H.-T. Wu, and C.-K. Sun, "Assessment of subtle changes in diabetes-associated arteriosclerosis using photoplethysmographic pulse wave from index finger," *J. Med. Syst.*, vol. 42, no. 3, p. 43, Mar. 2018.

[29] Y. Maeda, M. Sekine, and T. Tamura, "The advantages of wearable green reflected photoplethysmography," *J. Med. Syst.*, vol. 35, no. 5, pp. 829–834, Oct. 2011.

[30] E. Lee and C.-Y. Lee, "PPG-based smart wearable device with energy-efficient computing for mobile health-care applications," *IEEE Sensors J.*, vol. 21, no. 12, pp. 13564–13573, Jun. 2021.

[31] D. F. Swinehart, "The Beer–Lambert law," *J. Chem. Educ.*, vol. 39, no. 7, p. 333, 1962.

[32] S. Chatterjee and P. Kyriacou, "Monte Carlo analysis of optical interactions in reflectance and transmittance finger photoplethysmography," *Sensors*, vol. 19, no. 4, p. 789, Feb. 2019.

[33] C.-T. Yen, U.-H. Chen, G.-C. Wang, and Z.-X. Chen, "Non-invasive blood glucose estimation system based on a neural network with dual-wavelength photoplethysmography and bioelectrical impedance measuring," *Sensors*, vol. 22, no. 12, p. 4452, Jun. 2022.

[34] L. A. Castro-Pimentel, A. D. C. Téllez-Anguiano, O. I. Coronado-Reyes, and J. L. Diaz-Huerta, "Three-wavelength PPG and support vector machine for non-invasive estimation of blood glucose," *Opt. Quantum Electron.*, vol. 55, no. 8, p. 708, Aug. 2023.

[35] H. Tomiyama et al., "Influences of age and gender on results of noninvasive brachial–ankle pulse wave velocity measurement—A survey of 12517 subjects," *Atherosclerosis*, vol. 166, no. 2, pp. 303–309, Feb. 2003.

[36] B. K. Ha et al., "Relationships between brachial-ankle pulse wave velocity and peripheral neuropathy in type 2 diabetes," *Diabetes Metabolism J.*, vol. 36, no. 6, pp. 443–451, Dec. 2012.

[37] J.-A. Im, J.-W. Lee, J.-Y. Shim, H.-R. Lee, and D.-C. Lee, "Association between brachial-ankle pulse wave velocity and cardiovascular risk factors in healthy adolescents," *J. Pediatrics*, vol. 150, no. 3, pp. 247–251, Mar. 2007.

[38] R. W. van der Meer et al., "Magnetic resonance assessment of aortic pulse wave velocity, aortic distensibility, and cardiac function in uncomplicated type 2 diabetes mellitus," *J. Cardiovascular Magn. Reson.*, vol. 9, no. 4, pp. 645–651, 2007.
[39] Y.-X. Wang and R. Fitch, "Vascular stiffness: Measurements, mechanisms and implications," *Current Vascular Pharmacol.*, vol. 2, no. 4, pp. 379–384, Oct. 2004.
[40] Y. Li, X.-X. Tian, T. Liu, and R.-T. Wang, "Association between whole blood viscosity and arterial stiffness in patients with type 2 diabetes mellitus," *Endocrine*, vol. 49, no. 1, pp. 148–154, May 2015.
[41] S. J. Synowski, W. J. Kop, Z. S. Warwick, and S. R. Waldstein, "Effects of glucose ingestion on autonomic and cardiovascular measures during rest and mental challenge," *J. Psychosomatic Res.*, vol. 74, no. 2, pp. 149–154, Feb. 2013.
[42] W. Wang, S. Redline, and M. C. Khoo, "Autonomic markers of impaired glucose metabolism: Effects of sleep-disordered breathing," *J. Diabetes Sci. Technol.*, vol. 6, no. 5, pp. 1159–1171, 2012.
[43] J. Lee et al., "The effect of oral glucose tolerance testing on changes in arterial stiffness and blood pressure in elderly women with hypertension and relationships between the stage of diabetes and physical fitness levels," *Phys. Activity Nutrition*, vol. 24, no. 4, pp. 34–43, Dec. 2020.
[44] K. M. Choi et al., "Relationship between brachial-ankle pulse wave velocity and cardiovascular risk factors of the metabolic syndrome," *Diabetes Res. Clin. Pract.*, vol. 66, no. 1, pp. 57–61, Oct. 2004.
[45] H. Ohnishi et al., "Pulse wave velocity as an indicator of atherosclerosis in impaired fasting glucose," *Diabetes Care*, vol. 26, no. 2, pp. 437–440, Feb. 2003.

Po-Lei Lee (Member, IEEE) was born in 1973. He received the B.S. degree in electrical engineering from the National Cheng Kung University, Tainan, Taiwan, in 1995, and the Ph.D. degree from the Institute of Biomedical Engineering, National Yang-Ming University, Hsinchu, Taiwan, in 2000.

From 2001 to 2005, he was a Postdoctoral Fellow with the Taipei Veterans General Hospital, New Taipei, Taiwan, researching the signal and image-analysis procedures for electroencephalography and magnetoencephalography signals. He joined the Department of Electrical Engineering, National Central University, Taoyuan, Taiwan, in 2005, where he is currently a Distinguished Professor. He is also the Associated Dean of the College of Electrical and Computer Science, National Central University. His research interests include signal and image processing of biomedical signal processing, wearable devices, EEG and MEG signals as well as designing the EEG-based brain–computer interfaces.

Kuo-Wei Wang was born in 1969. He received the M.S. degree from Yuanpei University, Hsinchu, Taiwan, in 2007, and the Ph.D. degree in electrical engineering from the National Central University, Taoyuan, Taiwan, in 2019.

From 1981 to 2013, he worked at the Landseed International Hospital, Taoyuan, Taiwan, as the Director of the General Affair. His current research interests include magnetic resonance imaging and fMRI image analysis. He also interested in near infra-ray signal processing.

Chen-Yuan Hsiao was born in 1981. He received the M.D. degree from the Medical College, National Defense Medical Center, Taipei, Taiwan, in 2006, and the Ph.D. degree from the Graduate Institute of Medical Sciences, National Defense Medical Center, in 2020.

From 2006 to 2011, he was a resident with the Department of Surgery and had a fellowship in the Division of Cardiovascular Surgery, Taipei Veterans General Hospital, New Taipei, Taiwan. Since 2021, he has been an Attending Physician with the Division of Cardiovascular Surgery, Department of Surgery, Taipei Medical University Hospital, Taipei.